Modelled palaeolatitudes for the Louisville hot spot and the Ontong Java Plateau

MARIA ANTRETTER[1], PETER RIISAGER[2], STUART HALL[3], XIXI ZHAO[4] & BERNHARD STEINBERGER[5]

[1]*Department of Earth and Environmental Sciences, University of Munich, Theresienstrasse 41, D-80333 München, Germany (e-mail: maria@geophysik.uni-muenchen.de)*

[2]*Danish Lithosphere Centre, Øster Voldgade 10, DK-1350 Copenhagen K, Denmark*

[3]*Department of Geosciences, University of Houston, Houston, TX 77204-5007, USA*

[4]*Earth Sciences Department, University of California at Santa Cruz, Santa Cruz, CA 95064, USA*

[5]*IFREE, JAMSTEC, 2-15 Natsushima-cho, Yokosuka 237–0061, Japan*

Abstract: Formation of the Ontong Java Plateau (OJP), a large igneous province in the western Pacific, has been attributed to a rising plume head in the initial stage of the Louisville hot spot, approximately 120–125 Ma ago. However, the Neal *et al.* plate reconstruction suggests that the plateau formed approximately 9° north of the current location of this hot spot at 51°S . The magnetization of the plateau's basement records a palaeolatitude of approximately 25°S which further increases the discrepancy with the plume-head model. Modelling the motion of the Louisville hot spot for the last 120 Ma yields a possible southward motion of up to about 6°. True polar wander (TPW) models also shift the predicted palaeolatitudes of the plateau farther north. Taking into account both hot-spot motion and TPW, formation of the OJP by the Louisville hot spot remains a possibility.

The Ontong Java Plateau (OJP) in the western Pacific is the largest of the large igneous provinces (LIPs). Ar–Ar dating of basalts from the plateau indicates that it started to form approximately 120 Ma ago (Mahoney *et al.* 1993; Chambers *et al.* 2003). Most current models ascribe oceanic plateaus to the initial 'plume-head' stage of hot-spot development (e.g. Richards 1991). Richards (1991) and Tarduno *et al.* (1991) favoured the initial plume head of the Louisville hot spot (now at 51°S, 138°W) as the source of the OJP, but recent plate reconstructions suggest that the plateau was formed well to the NE of the current location of this hot spot (Neal *et al.* 1997; Kroenke *et al.* 2004). According to these reconstructions, the centre of the OJP at approximately 125 Ma was at 42°S, 159°W, and therefore 9° north and 21° west of the Louisville hot spot, approximately 1600 km distant (Fig. 1). This reconstruction is partly based on hot-spot tracks (including Louisville) and would therefore change if hot-spot motions were considered. The most recent palaeomagnetic results confirm that the OJP was far north of the present position of the Louisville hot spot at the time of the plateau's formation. Palaeomagnetic investigations on basalts from ODP Leg 192 to the OJP result in a palaeolatitude of $23.8\ ^{-2.0}/_{+1.9}$°S for the centre of the OJP 120 Ma ago (Riisager *et al.* 2003). These results have been combined with the palaeomagnetic investigation of volcaniclastic sediments from ODP Leg 192, resulting in a palaeolatitude of approximately 25°S (Riisager *et al.* 2004).

Mantle plumes have frequently been thought to be fixed in the Earth's mantle. If true polar wander (TPW) does not occur and the geomagnetic axial dipole hypothesis holds, then basalts from stationary mantle plumes would always be produced at the same place in the hot-spot reference frame as well as in the magnetic reference frame. Apart from palaeosecular variations, fresh basalts would always memorize the same direction of magnetization when cooling below their blocking temperature, corresponding to the present hot-spot latitude. Previous palaeomagnetic investigations (Mayer & Tarduno 1993) and the palaeomagnetic results from ODP Leg 192 to the OJP (Riisager *et al.* 2003, 2004) are inconsistent with these assumptions. Explanations for a discrepancy between palaeolatitudes and present-day hot-spot latitude include:

From: FITTON, J. G., MAHONEY, J. J., WALLACE, P. J. & SAUNDERS, A. D. (eds) 2004. *Origin and Evolution of the Ontong Java Plateau*. Geological Society, London, Special Publications, **229**, 21–30. 0305-8719/$15.00

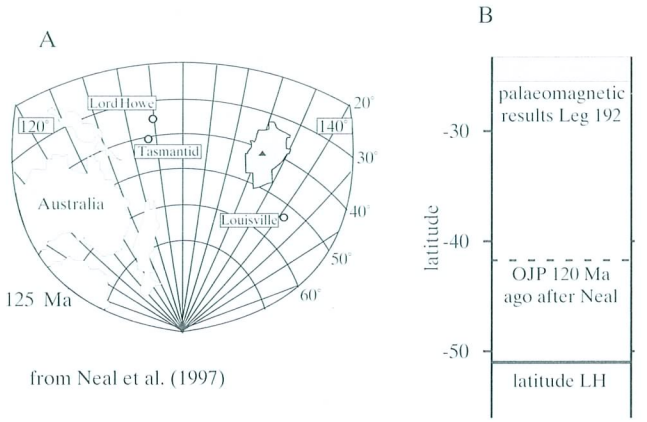

Fig. 1. (**A**) Approximate location of the Ontong Java Plateau (OJP) at 125 Ma after the plate reconstruction of Neal *et al.* (1997). The triangle represents the inferred location of the OJP plume centre beneath the crest of the high plateau. The reconstruction uses the Pacific plate Euler poles of Kroenke & Wessel (1997) (after Neal *et al.* 1997). (**B**) Sketch presenting the discrepancy between the present-day latitude of the Louisville hot spot, the latitude of the OJP 120 Ma ago after Neal *et al.* (1997) and the palaeolatitudes obtained by recent palaeomagnetic investigations on basalts from the OJP.

- mantle plumes can be advected when rising through the convecting mantle, resulting in hot-spot motion on the Earth's surface (e.g. Steinberger & O'Connell 1998);
- TPW, the relative motion between the mantle (with the hot spots) and the rotation axis of the Earth, may affect the latitude of a hot spot;
- non-dipole geomagnetic field components may contribute significantly to the Earth's magnetic field (e.g. Coupland & Van der Voo 1980; McElhinny *et al.* 1996) yielding palaeolatitudes that differ from those predicted by a dominantly geo-axial dipole (GAD) field.

Torsvik *et al.* (2001) and Van der Voo & Torsvik (2001) state that the octupole component is the most dominant non-dipole component. Introducing octupole contributions would rectify the latitude offset that is observed between the Louisville hot spot and the palaeomagnetic results from the OJP. Estimates of the magnitude of the octupole/dipole ratio indicate that paleolatitudes determined with the dipole formula could be about 7.5° too low at mid-latitudes (e.g. Van der Voo & Torsvik 2001).

In this chapter, we continue the discussion of the possible link between the OJP and the Louisville hot spot. We study the effect of a moving Louisville hot spot and the effect of TPW on palaeolatitudes, and discuss the consequence for the possible link between plateau and hot spot. However, there will be no further discussion of any contributions made by octupole fields.

Modelling of hot-spot motion

The motion of mantle plumes in a convecting mantle due to large-scale mantle flow can be estimated by geodynamic modelling (Steinberger & O'Connell 1998). The method that we use for the calculation has been previously explained in detail (Steinberger & O'Connell 1998, 2000; Steinberger 2000*a*; Antretter *et al.* 2002) and is briefly described here.

A large-scale mantle flow field is computed (Hager & O'Connell 1979, 1981) using models of internal density heterogeneities and surface plate motions. Density heterogeneities are inferred from seismic tomography or subduction history. For the scaling factors $(\delta\rho/\rho)/(\delta v_s/v_s)$ to convert seismic velocity (v) to present-day density (ρ) variations, we consider three cases: (1) scaling factor 0.2, where only mantle density anomalies below 220 km depth are included; (2) scaling factor 0.3, where only mantle density anomalies below 220 km depth are included; and (3) scaling factor 0.2, where all mantle density anomalies are included. A scaling factor between about 0.2 and 0.3 has been inferred from laboratory experiments, in combination with theoretical arguments (e.g. Karato 1993). Cases (1) and (2) disregard the uppermost 220 km in order to exclude seismic velocity variations that may be due to lithospheric roots and not therefore related to density variations that drive mantle flow. In most cases density variations are advected in the flow field backward in time for the past 68 Ma.

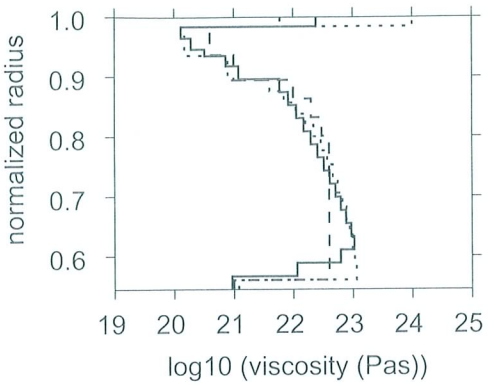

Fig. 2. Three radial viscosity models used in this paper. Dashed line, 'model A' (Steinberger & O'Connell 1998); dotted line, 'model B' (Steinberger & O'Connell 2000); continuous line, 'model C' (Steinberger & Calderwood 2001).

In most cases, relative plate motions are adopted from Mueller *et al.* (1993, 1997); for plates and times not included there or before 83 Ma, we follow Gordon & Jurdy (1986) (0–64 Ma) and Lithgow-Bertelloni *et al.* (1993) (64–120 Ma). Absolute motions of the African and Pacific plates are re-determined for times 0–74 Ma. We also re-computed plate boundaries in the Pacific Basin in 2 Ma intervals during the past 120 Ma based on the digital isochrons of Mueller *et al.* (1997), available online at ftp://ftp.agg.nrcan.gc,ca/products/agegrid/isochrons.dat.gz. Elsewhere, plate boundary locations are adopted from the compilation by Lithgow-Bertelloni *et al.* (1993).

The inferred past plate boundary locations in the Pacific Basin depend on the 'absolute' plate motions, which in turn depend on hot-spot motion. In principle, it requires an iteration to obtain mutually consistent hot-spot motions, plate motions and plate boundaries (Tarduno *et al.* 2003). Here, for simplicity, we use the same plate motions and boundaries that were computed for *one specific* model of hot-spot motion – the 'moving source' model of Tarduno *et al.* (2003) – that yields a good fit to Pacific hot-spot tracks. This procedure is appropriate as, for models of hot-spot motion that yield a good fit to both the Hawaiian and Louisville hot-spot track, the Louisville hot spot is located in an intra-plate location on the Pacific plate. Except for the very recent past, the Louisville hot spot is located far away from plate boundaries and, as long as this is the case, the computed Louisville hot-spot motion depends very little on the exact plate boundary conditions.

Furthermore, radial mantle viscosity structures (Steinberger & O'Connell 1998, 2000; Steinberger & Calderwood 2001) are assumed for the calculations. These are shown in Figure 2, and will be referred to as viscosity models A, B and C.

Most models were computed for an incompressible mantle without phase boundaries. Some models consider compressibility and phase boundaries, as in Steinberger (2000*a*). In particular, if phase boundaries are considered, they are assumed to be in thermal equilibrium. Density anomalies at the depth of the phase boundaries inferred from three-dimensional (3-D) tomography models are converted to temperature anomalies which, in turn, are converted to phase boundary deflections that are treated as sheet mass anomalies. Based on the work of Akaogi *et al.* (1989) and Akaogi & Ito (1999) we use conversion factors from density to sheet mass anomalies of 132 km at depth 400 km and –58 km at depth 670 km. Roughly speaking, this means that a density anomaly layer of thickness 132 km around 400 km depth is counted twice, whereas a density layer of 58 km thickness at depth 670 km is disregarded. To calculate the motion of hot spots, we assume that initially (for the Louisville hot spot, at 120 Ma) vertical plume conduits are subsequently distorted in large-scale mantle flow. Besides being distorted in large-scale flow we also allow for buoyant 'Stokes' rising of plume conduits through mantle flow. The resulting hot spot motion depends on both the large-scale flow field and the buoyant rising of the plume conduit. Buoyant rising velocity is computed from a modified Stokes formula: $u(z) = u_0 \times (r/r_0)^2 \times (\eta_0/\eta(z))$, where $u_0 = 51$ mm year^{-1}, $r_0 = 100$ km, $\eta_0 = 10^{21}$ Pa s, z is the depth, $\eta(z)$ is the ambient mantle viscosity and r is plume conduit radius. The value $u_0 = 51$ mm year^{-1} corresponds to rising speed obtained in laboratory experiments (Richards & Griffiths 1988) scaled to Earth dimensions, and for a reasonable density contrast of 30 kg m^{-2} between plume and ambient mantle.

We use three different assumptions about plume conduit radius.

(1) Independent of depth, $r = (B/B_0)^{1/4} \times r_1$, where B is anomalous plume mass flux, $B_0 = 10^3$ kg s^{-1}, and $r_1 = 41.0$ km for viscosity models B and C (i.e. most cases), and $r_1 = 62.5$ km for model A. This assumption follows Steinberger (2000*a*) and Steinberger & O'Connell (2000), where it is further discussed.

(2) Dependent on depth, $r = ((B/B_0) \times (\eta(z)/\eta_0))^{1/4} \times r_1$ with $r_1 = 65.9$ km for viscosity model B and 68.2 km for model C – such that conduit radius immediately

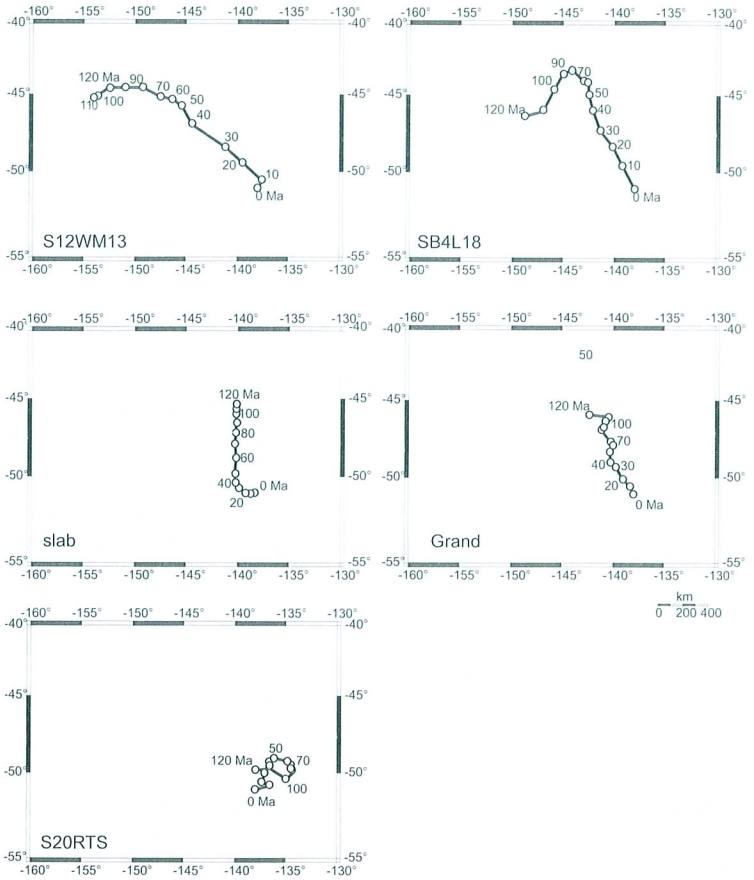

Fig. 3. Modelled drift of the Louisville hot spot assuming its initiation at 120 Ma. The dots give the position of the hot spot every 10 Ma, indicated also by numbers. The present-day position of the Louisville hot spot is assumed at 51°S at 0 Ma. The tomographic models S12WM13 (Su *et al.* 1994) and SB4L18 (Masters *et al.* 2000), and the slab model of Steinberger (2000*b*), have been used in combination with mantle viscosity model B to obtain a mantle flow field in which the rising mantle plume is advected; the tomographic models of Grand (2002) and S20RTS (Ritsema & Van Heijst 2000) have been used with viscosity model C.

below the lithosphere is again 41.0 km for $B = B_0$. This corresponds to assuming relative viscosity variations with depth inside the conduit are the same as in the ambient mantle.

(3) Dependent on depth, $r = ((B/B_0) \times (\eta(z)/\eta_0))^{1/4} \times r_1 + r_{th}$, with $r_1 = 21.6$ km and $r_{th} = 40$ km. Different from (2), the conduit is surrounded by a 'thermal halo' of thickness r_{th}. This assumption is intermediate between (1) and (2).

We use $B = 2.0 \times 10^3$ kg s^{-1}, the average between 0.9×10^3 kg s^{-1} (Sleep 1990) and 3.0×10^3 kg s^{-1} (Davies 1988). Computations were also carried out for these two values, which produced very similar results.

We assume a present hot-spot location at 50.9°S, 138.1°W, such that the predicted track approximately matches location (50.4°S, 139.2°W) and age 0.5 ± 0.2 Ma (Watts *et al.* 1988) of the youngest seamount of the Louisville chain. This location is also supported by geochemical evidence (Vlastelic *et al.* 1998), but differs from the location (53.8°S, 140.2°W) proposed by Wessel & Kroenke (1997).

Results: motion of the Louisville hot spot

Some representative results for hot-spot motion are shown in Figure 3. The tomographic models S12WM13 (Su *et al.* 1994) and SB4L18 (Masters *et al.* 2000), and the slab model of Steinberger (2000*b*), have been used in combination with

Table 1. *Parameters and results of numerical model runs, in addition to those where results are displayed in Figure 3*

#	TM	SF	MVM	PVM	td	adv	com	pb	HS120 (long.)	HS120 (lat.)
1	1	1	A	1	y	y	n	n	−149.4	−50.2
2	1	1	A	1	y	y	y	n	−150.1	−51.1
3	1	1	A	1	y	y	n	y	−149.1	−50.7
4	1	1	B	1	y	y	n	n	−147.3	−48.5
5	1	3	B	1	y	y	n	n	−153.4	−45.1
6	1	1	B	1	y	n	n	n	−140.2	−45.9
7	1	1	B	1	n	n	n	n	−144.0	−45.3
8	1	1	C	1	y	y	n	n	−151.1	−50.5
9	1	1	C	2	y	y	n	n	−138.4	−52.3
10	1	1	C	3	y	y	n	n	−146.5	−51.1
11	2	1	B	1	y	y	n	n	−148.1	−46.0
12	2	1	B	2	y	y	n	n	−142.6	−45.7
13	2	1	C	1	y	y	n	n	−151.4	−48.2
14	2	1	C	1	y	y	y	y	−151.3	−50.6
15	2	1	C	1	y	n	n	n	−146.8	−42.3
16	2	2	C	1	y	y	n	n	−154.3	−50.2
17	2	2	C	1	y	y	y	n	−155.8	−52.6
18	2	3	C	1	y	y	n	n	−158.4	−44.7
19	2	3	C	1	y	n	n	n	−146.8	−42.0

Abbreviations: #, model case number. TM, tomography model: 1, S12WM13 (Su *et al.* 1994); 2, SB4L18 (Masters *et al.* 2000). SF, scaling factors $(\delta\rho/\rho)/(\delta v_s/v_s)$ to convert seismic velocity to density variations: 1, scaling factor 0.2, only mantle density anomalies below 220 km depth are included; 2, scaling factor 0.3, only mantle density anomalies below 220 km depth are included; 3, scaling factor 0.2, all mantle density anomalies are included. MVM, mantle viscosity model (see text): A, Steinberger (2000); B, Steinberger & O'Connell (1998); C, Steinberger & Calderwood (2001). PVM, plume viscosity model: 1, viscosity inside plume conduit and plume conduit radius are constant; plume conduit rising speed is inversely proportional to viscosity of the mantle surrounding the conduit; 2, viscosity inside plume conduit and plume conduit radius increase with depth; plume conduit rising speed is inversely proportional to the square root of viscosity of the mantle surrounding the conduit; 3, viscosity inside plume conduit and plume conduit radius increase with depth; plume conduit is surrounded by a thermal halo (see text for more details). td, time-dependent plate motion boundary condition (y/n) (y, as explained in the text; n, constant present-day plate motions and boundaries). adv, advection of density heterogeneities for 68 Ma (y/n). com, compressible mantle (y/n). pb, phase boundaries (y/n). HS120, computed hot-spot location (°) at 120 Ma.

mantle viscosity model B to obtain a mantle flow field in which the rising mantle plume is advected. The tomographic models of Grand (2002; an updated model based on Grand *et al.* 1997) and S20RTS (Ritsema & Van Heijst 2000) have been used with viscosity model C. The first scaling factor relation (including only density anomalies below depth 220 km) is used in all cases except in combination with S12WM13 (Su *et al.* 1994), where the third relation (including all density anomalies, as in Steinberger & O'Connell 1998) is used. All cases shown are for an incompressible mantle without phase boundaries, time-dependent plate motion boundary conditions, backwards advection of density heterogeneities as explained and the first assumption about plume conduit radius.

Calculations yield a southward motion of 5° for the model based on SB4L18 (Masters *et al.* 2000) and 6° for the model based on S12WM13 (Su *et al.* 1994), and the slab model of Steinberger (2000*b*). The calculations with SB4L18 (Masters *et al.* 2000) and S12WM13 (Su *et al.* 1994) give approximately 10° and 15° eastward motion, respectively. The former gives a position of the hot spot 120 Ma ago at 45°S and 153°W, very close to the centre of the OJP at the same time, according to the plate reconstruction of Neal *et al.* (1997). However, the two positions cannot be directly compared, as the reconstruction of Neal *et al.* (1997) is based on the assumption of hot-spot fixity. The hot spot moves approximately 5° southward and 4° eastward using the model of Grand (2002), and total motion is only about 1° southward and 1° eastward when using the tomographic model of Ritsema & Van Heijst (2000). To test the effect of other modelling assumptions on our results, several input parameters have been varied for two representative tomographic input models (Su *et al.* 1994; Masters *et al.* 2000), and the results are shown in Table 1.

Discussion

Motion of plume conduits in our model is dominated by advection in the lower part of the mantle, and buoyant rising in the upper part of the mantle. Thus, computed surface hot-spot motion is frequently similar to flow at mid-mantle depth (i.e. upper part of the lower mantle) where the transition between 'low' and 'high' viscosity occurs (Steinberger & O'Connell 2000). All flow models considered show downward flow surrounding the Pacific, and a large-scale upwelling beneath the Pacific, which tends to be more focused for the models based on tomography and more diffuse for the one based on subduction history. Horizontal flow at mid-mantle depth has an outward flow component away from the large-scale upwelling, which is southward in the area of the Louisville hot spot. Another component is plate return flow towards the Pacific–Antarctic ridge, which is southeastward in this area for more recent times. Thus, from these two flow components we can qualitatively expect a southward component of Louisville hot-spot motion, but its speed should not exceed horizontal flow speeds at mid-mantle depths (*c.* 1 cm year^{-1}).

Details of mantle density structure in the south Pacific are not well known, hence there are considerable differences among models of flow and hot-spot motion (Fig. 2). For the present-day flow fields computed for models S12WM13 and SB4L18, the large upwelling beneath the Pacific is connected with a regional upwelling SE of New Zealand, SW of the Louisville hot spot. This yields, for those cases where advection of density heterogeneities is not considered, a mid-mantle flow in a SE direction, superimposed on plate return flow in the same direction that results in a SE motion of the hot spot. If density anomalies derived from these two tomography models are advected back in time, the upwelling SE of New Zealand tends to become stronger and a NE hot-spot motion is predicted for older times (Fig. 2A and C). Thus, in cases 4, 13 and 18 of Table 1, which include advection, the total southward hot-spot motion is less than in the corresponding cases 6, 15 and 19 without advection.

Comparison between cases 6 and 7 of Table 1 shows the effect of different plate motion boundary conditions. More recently, the hot spot has been closer to the ridge, hence more affected by (SE) plate return flow than in the more distant past. Hence, using constant present-day boundary conditions yields stronger hot-spot motion.

Comparison between cases 1–3, 13 and 14, as well as 16 and 17, shows that considering phase boundaries and compressibility leads to a predicted hot-spot location farther south at 120 Ma. Comparison between cases 4 and 5, as well as 13, 16 and 18, shows the effect of different scaling factors. Stronger density anomalies lead to stronger flow and hence more hot-spot motion. Comparison between cases 1, 4 and 8, as well as 11 and 13, shows the effect of radial ambient mantle viscosity structure. Comparison between cases 8–10, as well as 11 and 12, shows the effect of different buoyant plume rising speed. In the cases with higher rising speed, the computed total hot-spot motion tends to be less, but with a variable effect on the N–S component.

Altogether, in Figure 3 and Table 1, hot-spot motion varies between 9° southward (6° if we only count cases that consider advection of density heterogeneities) and 1° northward. The result used by Tarduno *et al.* (2003), which was obtained for a 'mean' tomography model, is also within that range.

Obviously, it is also possible to construct models with substantially larger Louisville hot-spot motion (e.g. Steinberger & O'Connell 1998); however, such models are not consistent with observations, such as hot-spot tracks globally, whereas our calculations suggest that all model parameters used here are broadly consistent with global observations.

In contrast to mid-mantle flow, flow at the base of the mantle is mostly towards large-scale and regional upwellings. Thus, in our model, plume conduits tend to get tilted, with their bases closer to these upwellings than the top. If such a tilted conduit rises to the surface it straightens up again, and in the process moves *towards*, rather than away from, the upwelling. This effect is, for example, responsible for the change in direction of hot-spot motion computed during the past 10 Ma for the model using S12WM13, shown in Figure 2. However, motion away from lower-mantle upwellings tends to occur far more frequently in our models for the Louisville hot spot. Frequently, a rather strong tilt is computed for the Louisville plume conduit for the past few 10 Ma. In the real mantle, a strongly tilted plume conduit might not remain intact but break up into several drops (Whitehead 1982). A strong tilt may be responsible for Louisville hot-spot volcanism becoming rather episodic during the more recent past, producing individual seamounts with larger spacing.

In contrast, Tarduno *et al.* (2003) discussed how straightening up of a tilted conduit may have caused rapid southward motion of the Hawaiian hot spot, i.e. motion *towards* the large-scale upwelling. Qualitatively, a number of

reasons can be given why this may have happened for Hawaii, but not for Louisville:

- the Hawaiian plume is stronger, hence has higher buoyancy and a greater tendency to straighten up;
- the Hawaiian plume may be older and, hence, in a stage of straightening up again, whereas the Louisville hot spot may have not yet reached that stage;
- because the flow field related to the large-scale upwelling under the central Pacific is superposed on plate return flow, which is in a SE direction beneath both hot spots, the transition from flow towards the upwelling to flow away from the upwelling occurs at a shallower depth in the case of Hawaii. Hence, the Hawaiian hot spot is more likely to move towards the upwelling than the Louisville hot spot.

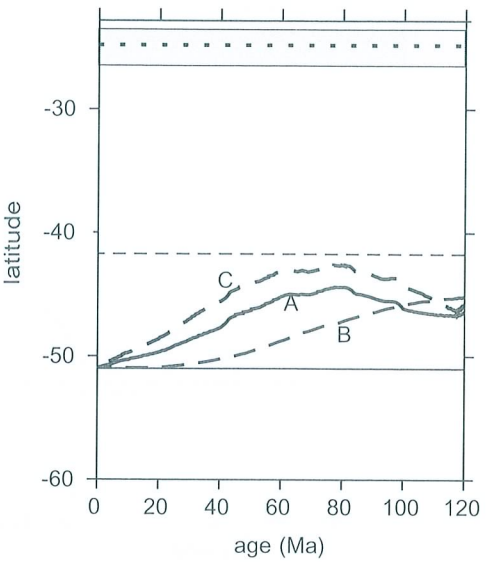

Fig. 4. Palaeolatitudes v. time for the Louisville hot spot for models that give southward hot-spot motion. A, Su *et al.* (1994); B, Steinberger (2000*b*); and C, Masters *et al.* (2000). The estimated present-day position of the Louisville hot spot, as well as the centre of the OJP suggested by Neal *et al.* (1997), are indicated by a solid and dashed horizontal line, respectively. The palaeomagnetically determined palaeolatitude and uncertainties are represented by the shaded area.

Effect of hot-spot motion on palaeolatitudes

Figure 4 shows the palaeolatitudes for the Louisville hot spot v. time for some of the calculations shown in Figure 3, which yield appreciable southward motion. For comparison, the horizontal dashed line indicates the centre of the plateau 120 Ma ago, as suggested by Neal *et al.* (1997). A southward motion of the hot spot could explain a large part of the discrepancy between the plate reconstruction of Neal *et al.* (1997) and the Louisville hot-spot latitude. However, its amount is not large enough to explain the low palaeolatitude of approximately 25°S obtained by Riisager *et al.* (2003, 2004) from basalts and volcaniclastic sediments from the OJP.

Effect of TPW on palaeolatitudes

True polar wander is defined as the relative motion between the Earth's mantle and the rotation axis of the Earth. The most recent TPW curves by Prévot *et al.* (2000) and Besse & Courtillot (2002) both use a fixed hot-spot reference frame. As discussed previously (Antretter *et al.* 2002), this should be modified if hot-spot motion is considered. However, we found that for models similar to the one shown here such a modification produces no more than a 2° difference. To keep the model simple we therefore did not implement such a modification.

The change in hot-spot latitude with time that results from TPW is shown in Figure 5. For both TPW curves the effect on the latitude is small for the past *c.* 100 Ma. Prior to that, TPW provides palaeolatitudes for the Louisville hot spot up to 11° farther north than the present-day hot-spot position (Fig. 5), thus further reducing the discrepancy between the present-day latitude of the Louisville hot spot and the recent palaeomagnetic results from the OJP.

Conclusion

Recent palaeomagnetic results from the OJP (Riisager *et al.* 2003, 2004) yield a palaeolatitude of approximately 25°S, whereas the present-day latitude of the Louisville hot spot is approximately 51°S. The effect of TPW on the palaeolatitudes can explain up to 11° of this difference. Our models for the motion of the Louisville hot spot yield up to 6° of southward motion (9°, if present-day density heterogeneities are used for all times), depending on the tomographic models and parameters used. Taking into account both TPW and hot-spot motion, and considering the largest southward shifts resulting from both

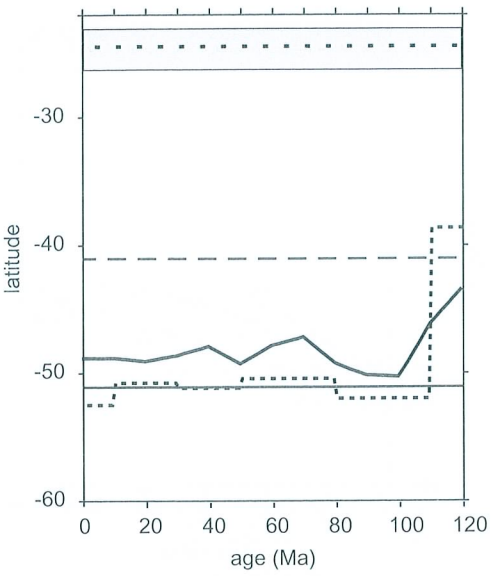

Fig. 5. The effect of TPW on the palaeolatitude of the Louisville hot spot for two different TPW paths (solid line, Besse & Courtillot 2002; dotted line, Prévot *et al.* 2000). The centre of the OJP suggested by Neal *et al.* (1997) and the palaeomagnetically determined palaeolatitude (with uncertainties) are shown as a dashed horizontal line and a shaded area, respectively.

effects, we can explain a latitudinal shift of approximately 17°–20°. Considering the effect of long-term octupole contributions may explain an additional shift of approximately 7.5° . Thus, a favourable combination of all three effects is just sufficient to explain the discrepancy of approximately 26° between the palaeomagnetic results and the present-day hot-spot position. Thus, it remains possible that the Louisville hot-spot was the source of the OJP.

Funding for this research was provided by the Deutsche Forschungsgemeinschaft DFG, ODP/Germany, Project Number So72/70–1 (M. Antretter, B. Steinberger), the Danish National Research Foundation (P. Riisager), US Science Support Program of JOI (S. Hall), and NSF grants EAR 443549–22178 and EAR 443747–22250 (X. Zhao). The authors would like to thank the crew and scientific party of ODP Leg 192 for their invaluable work and comments.

References

AKAOGI, M. & ITO, E. 1999. Calorimetric study on majorite–perovskite transition in the system $Mg_4Si_4O_{12}$–$Mg_3Al_2Si_3O_{12}$: transition boundaries with positive pressure–temperature slopes. *Physics of the Earth and Planetary Interiors*, **114**, 129–140.

AKAOGI, M., ITO, E. & NAVROTSKY, A. 1989. Olivine-modified spinel–spinel transitions in the system Mg_2SiO_4–Fe_2SiO_4: Calorimetric measurements, thermochemical calculations, and geophysical application. *Journal of Geophysical Research*, **94**, 15 671–15 685.

ANTRETTER, M., STEINBERGER, B., HEIDER, F. & SOFFEL, H. 2002. Paleolatitudes of the Kerguelen hotspot: new paleomagnetic results and dynamic modeling. *Earth and Planetary Science Letters*, **203**, 635–650.

BESSE, J. & COURTILLOT, V. 2002. Apparent and true polar wander and the geometry of the geomagnetic field in the last 200 Myr. *Journal of Geophysical Research*, **107**, 2300. doi: 10.1029/2000JB000050.

CHAMBERS, L., PRINGLE, M. & FITTON, G. 2003. Age and duration of magmatism on the Ontong Java Plateau. *Geophysical Research Abstracts*, **5**, 09657.

COUPLAND, D.H. & VAN DER VOO, R. 1980. Long-term non-dipole components in the geomangetic field during the last 130 m.y. *Journal of Geophysical Research*, **85**, 3529–3549.

DAVIES, G.F. 1988. Ocean bathymetry and mantle convection, 1, Large-scale flow and hotspots. *Journal of Geophysical Research*, **93**, 10 467–10 480.

GRAND, S.P., VAN DER HILST, R.D. & WIDIYANTORO, S. 1997. Global seismic tomography: A snapshot of convection in the Earth. *Geological Society of America*, **7**, 1–7.

GRAND, S.P. 2002. Available online at ftp: //bratsche.geo.utexas.edu/outgoing/steveg/.

GORDON, R.G. & JURDY, D. 1986. Cenozoic global plate motions. *Journal of Geophysical Research*, **91**, 12 389–12 406.

HAGER, B.H. & O'CONNELL, R.J. 1979. Kinematic models of large-scale mantle flow. *Journal of Geophysical Research*, **84**, 1031–1048.

HAGER, B.H. & O'CONNELL, R.J. 1981. A simple global model of plate dynamics and mantle convection. *Journal of Geophysical Research*, **86**, 4843–4867.

KARATO, S. 1993. Importance of anelasticity in the interpretation of seismic tomography. *Geophysical Research Letters*, **20**, 1623–1626.

KROENKE, L.W. & WESSEL, P. 1997. Pacific plate motion between 125 and 90 Ma and the formation of the Ontong Java Plateau (abstract). American Geophysical Union Chapman Conference on Global Plate Motions, Marshall, CA, **22**.

KROENKE, L.W., WESSEL, P. & STERLING, A. 2004. Motion of the Ontong Java Plateau in the hot-spot frame of reference: 122 Ma–present. *In*: FITTON, J.G., MAHONEY, J.J., WALLACE, P.J. & SAUNDERS, A.D. (eds) *Origin and Evolution of the Ontong Java Plateau*. Geological Society, London, Special Publications, **229**, 9–20.

LITHGOW-BERTELLONI, C., RICHARDS, M.A., RICARD, Y., O'CONNELL, R.J. & ENGEBRETSON, D.C. 1993.

Toroidal–poloidal partitioning of plate motions since 120 Ma. *Geophysical Research Letters*, **20**, 375–378.

MAHONEY, J.J., STOREY, M., DUNCAN, R.A., SPENCER, K. J. & PRINGLE, M. 1993. Geochemistry and geochronology of the Ontong Java Plateau. *In*: PRINGLE, M., SAGER, W., SLITER, W. & STEIN, S. (eds) *The Mesozoic Pacific: Geology, Tectonics, and Volcanism*. American Geophysical Union, Geophysical Monograph, **77**, 233–261.

MCELHINNY, M.W., MCFADDEN, P.L. & MERRILL, R.T. 1996. The time averaged paleomagnetic field 0–5 Ma. *Journal of Geophysical Research B: Solid Earth*, **101**, 25 007–25 028.

MUELLER, R.D., ROEST, W.R., ROYER, J.-Y., GAHAGAN, L.M. & SCLATER, J.G. 1997. Digital isochrons of the world's ocean floor. *Journal of Geophysical Research*, **102**, 3211–3214.

MUELLER, R.D., ROYER, J.-Y. & LAWVER, L.A. 1993. Revised plate motions relative to the hotspots from combined Atlantic and Indian Ocean hotspot tracks. *Geology*, **21**, 275–278.

MASTERS, G., LASKE, G., BOLTON, H. & DZIEWONSKI, A. 2000. The relative behaviour of shear velocity, bulk sound speed, and compressional velocity in the mantle: implications for chemical and thermal structure. *In*: KARATO, S. (ed.) *Seismology and Mineral Physics*. American Geophysical Union, Geophysical Monograph, **117**, 63–87.

MAYER, H. & TARDUNO, J.A. 1993. Paleomagnetic investigation of the igneous sequence, Site 807, Ontong Java Plateau, and a discussion of pacific true polar wander. *In*: BERGER, W.H., KROENKE, L.W., MAYER, L.A., *et al.* (eds) *Proceedings of ODP, Scientific Results*, **130**, 51–59, College Station, TX (Ocean Drilling Program).

NEAL, C.R., MAHONEY, J.J., KROENKE, L.W., DUNCAN, R.A. & PETTERSON, M.G. 1997. The Ontong Java Plateau. *In*: MAHONEY, J.J. & COFFIN, M.F. (eds) *Large Igneous Provinces: Continental, Oceanic and Planetary Flood Basaltic Volcanism*. American Geophysical Union, Geophysical Monograph, **100**, 183–216.

PRÉVOT, M., MATTERN, E., CAMPS, P. & DAIGNIÈRES, M. 2000. Evidence for a 20° tilting of the Earth's rotation axis 110 million years ago. *Earth and Planetary Science Letters*, **179**, 517–528.

RICHARDS, M.A. 1991. Hotspots and the case against a uniform viscosity composition mantle. *In*: SABADINI, R. & LAMBECK, K. (eds) *Glacial Isostasy, Sea Level and Mantle Rheology*. Kluwer, Dordrecht, 571–587.

RICHARDS, M.A. & GRIFFITHS, R.W. 1988. Deflection of plumes by mantle shear flow: Experimental results and a simple theory. *Geophysical Journal*, **94**, 367–376.

RICHARDS, M.A., JONES, D.L., DUNCAN, R.A. & DEPAOLO, D.J. 1991. A mantle plume initiation model for the Wrangellia flood basalt and other oceanic plateaus. *Science*, **254**, 263–267.

RIISAGER, P., HALL, S., ANTRETTER, M. & ZHAO, X. 2003. Paleomagnetic paleolatitude of Early Cretaceous Ontong Java Plateau Basalts: implications for pacific apparent and true polar wander. *Earth and Planetary Science Letters*, **208**, 235–252.

RIISAGER, P., HALL, S., ANTRETTER, M. & ZHAO, X. 2004. Early Cretaceous Pacific palaeomagnetic pole from Ontong Java Plateau basement rocks. *In*: FITTON, J.G., MAHONEY, J.J., WALLACE, P.J. & SAUNDERS, A.D. (eds) *Origin and Evolution of the Ontong Java Plateau*. Geological Society, London, Special Publications, **229**, 31–44.

RITSEMA, J. & VAN HEIJST, H.J. 2000. Seismic imaging of structural heterogeneity in Earth's mantle: Evidence for large-scale mantle flow. *Science Progress*, **83**, 243–259.

SLEEP, N. 1990. Hotspots and mantle plumes: Some phenomenology. *Journal of Geophysical Research*, **95**, 6715–6736.

STEINBERGER, B. 2000*a*. Plumes in a convecting mantle; models and observations for individual hotspots. *Journal of Geophysical Research*, **10**, 11 127–11 152.

STEINBERGER, B. 2000*b*. Slabs in the lower mantle – results of dynamic modelling compared with tomographic images and the geoid. *Physics of the Earth and Planetary Interiors*, **118**, 241–257.

STEINBERGER, B. & CALDERWOOD, A.R. 2001. Mineral physics constraints on viscous flow models of mantle flow. *Journal of Conference Abstracts*, Cambridge Publications, Abstracts for EUG XI, 423–424.

STEINBERGER, B. & O'CONNELL, R.D. 1998. Advection of plumes in mantle flow: implications for hotspot motion, mantle viscosity and plume distribution. *Geophysical Journal International*, **132**, 412–434.

STEINBERGER, B. & O'CONNELL, R.D. 2000. Effects of mantle flow on hotspot motion. *In*: RICHARDS, M.A., GORDEON, R.G. & VAN DER HILST, R.D. (eds) *The History and Dynamics of Global Plate Motions*. American Geophysical Union, Geophysical Monograph, **121**, 377–398.

SU, W.-J., WOODWARD, R.L. & DZIEWONSKI, A.M. 1994. Degree 12 model of shear velocity heterogeneity in the mantle. *Journal of Geophysical Research*, **99**, 6945–6980.

TARDUNO, J.A., DUNCAN, R.A., SCHOLL, D.W., COTTRELL, R.D., STEINBERGER, B., THORDARSON, T., KERR, B.C., NEAL, C.R., FREY, F.A., TORII, M. & CARVALLO, C. 2003. The Emperor Seamounts: Southward motion of the Hawaiian hotspot plume in Earth's mantle. *Science*, **301**, 1064–1069.

TARDUNO, J.A., SLITER, W.V., KROENKE, L.W., LECKIE, M., MAHONEY, J.J., MUSGRAVE, R.J., STOREY, M. & WINTERER, E.L. 1991. Rapid formation of the Ontong Java Plateau by Aptian mantle plume volcanism. *Science*, **254**, 399–403.

TORSVIK, T.H., MOSAR, J. & EIDE, E.A. 2001. Cretaceous–Tertiary geodynamics: A North Atlantic exercise. *Geophysical Journal International*, **146**, 850–867.

VAN DER VOO, R. & TORSVIK, T.H. 2001. Evidence for late Paleooic and Mesozoic non-dipole fields

provides an explanation for the Pangea reconstruction problems. *Earth and Planetary Science Letters*, **187**, 71–81.

VLASTELIC, I., DOSSO, L., GUILLOU, H., BOUGAULT, H., GELI, L., ETOUBLEAU, J. & JORON, J.L. 1998. Geochemistry of the Hollister Ridge: relation with the Louisville hotspot and the Pacific–Antarctic Ridge. *Earth and Planetary Science Letters*, **160**, 777–793.

WATTS, A.B., WEISSEL, J.K., DUNCAN, R.A. & LARSON, R.L. 1988. Origin of the Louisville Ridge and its relationship to the Eltanin Fracture Zone System. *Journal of Geophysical Research*, **93**, 3051–3077.

WESSEL, P. & KROENKE, L.W. 1997. A geometric technique for relocating hotspots and refining absolute plate motions. *Nature*, **387**, 365–369.

WHITEHEAD, J.A. 1982. Instabilities of fluid conduits in a flowing Earth – are plates lubricated by the asthenosphere? *Geophysical Journal of the Royal Astronomical Society*, **70**, 415–433.